DOT/FAA/AR-10/46

Air Traffic Organization
NextGen & Operations Planning
Office of Research and
Technology Development
Washington, DC 20591

Monitoring of Impact Damages in Adhesively Bonded Composites

January 2011

Final Report

This document is available to the U.S. public through the National Technical Information Services (NTIS), Springfield, Virginia 22161.

This document is also available from the Federal Aviation Administration William J. Hughes Technical Center at actlibrary.tc.faa.gov.

U.S. Department of Transportation
Federal Aviation Administration

NOTICE

This document is disseminated under the sponsorship of the U.S. Department of Transportation in the interest of information exchange. The United States Government assumes no liability for the contents or use thereof. The United States Government does not endorse products or manufacturers. Trade or manufacturer's names appear herein solely because they are considered essential to the objective of this report. The findings and conclusions in this report are those of the author(s) and do not necessarily represent the views of the funding agency. This document does not constitute FAA certification policy. Consult your local FAA aircraft certification office as to its use.

This report is available at the Federal Aviation Administration William J. Hughes Technical Center's Full-Text Technical Reports page: actlibrary.tc.faa.gov in Adobe Acrobat portable document format (PDF).

Technical Report Documentation Page

1. Report No.	2. Government Accession No.	3. Recipient's Catalog No.
DOT/FAA/AR-10/46		

4. Title and Subtitle	5. Report Date
MONITORING OF IMPACT DAMAGES IN ADHESIVELY BONDED COMPOSITES	January 2011
	6. Performing Organization Code
7. Author(s)	8. Performing Organization Report No.
Qiaojian Huang, Brad Regez, and Sridhar Krishnaswamy	
9. Performing Organization Name and Address	10. Work Unit No. (TRAIS)
Center for Quality Engineering and Failure Prevention Northwestern University Rm 327, 2137 Tech Drive Evanston, IL 60208, USA	11. Contract or Grant No. 04-C-AM-NWU
12. Sponsoring Agency Name and Address	13. Type of Report and Period Covered
U.S. Department of Transportation Federal Aviation Administration Air Traffic Organization NextGen & Operations Planning Office of Research and Technology Development Washington, DC 20591	Final Report 14. Sponsoring Agency Code ANM-115

15. Supplementary Notes

The Federal Aviation Administration Airport and Aircraft Safety R&D Division Technical Monitor was David Westlund.

16. Abstract

In this report, a photoacoustic technique was first applied to measure the dispersive property of a GLAss-REinforced (GLARE) aluminum composite panel. The measured phase velocity dispersion curves were consistent with the theoretical calculation using the classical transfer matrix method for layered media. Based on the obtained properties, a finite element model was constructed to study the influence of a disbond void on the Lamb wave propagation in the GLARE plate. It was found that both the displacement amplitudes and travel time of the A_0 mode Lamb waves showed distinct differences with and without the disbond, which can be used to monitor the disbond growth.

A series of experiments were carried out to study the influence of disbonds on Lamb wave propagation in the GLARE composites. Guided Lamb waves were launched and detected with polyvinylidene fluoride (PVDF) comb transducers. Disbond defects were introduced with a ball drop test to study their influence on the Lamb wave signals. The amplitudes of the detected Lamb wave signals showed distinct differences with and without disbonds. In addition, a thermal-imaging technique was applied to inspect the disbond region to cross-correlate the disbond size with its influence on the Lamb wave signals that were measured by the PVDF sensors. It was demonstrated that the A_0 mode Lamb wave amplitudes decreased exponentially as the disbond size increased. It was shown that the disbond defect sizes can be predicted from the measured Lamb wave signals using a simple exponential model.

17. Key Words	18. Distribution Statement
Disbond defect, Lamb waves, GLARE composites, Finite element method, Ball drop test, PVDF transducer	This document is available to the U.S. public through the National Technical Information Service (NTIS), Springfield, Virginia 22161. This document is also available from the Federal Aviation Administration William J. Hughes Technical Center at actlibrary.tc.faa.gov.

19. Security Classif. (of this report)	20. Security Classif. (of this page)	21. No. of Pages	22. Price
Unclassified	Unclassified	26	

Form DOT F 1700.7 (8-72) Reproduction of completed page authorized

TABLE OF CONTENTS

		Page
EXECUTIVE SUMMARY		vii
1.	INTRODUCTION	1
1.1	Background	1
1.2	Purpose	1
1.3	Report Overview	1
2.	EXPERIMENTS	2
2.1	Photoacoustic Technique	2
2.2	Lamb Wave Test	2
2.3	Ball Drop Test	4
2.4	Thermal-Imaging Technique	4
3.	THEORY	5
3.1	Dispersive Property of the GLARE Plate	5
3.2	Finite Element Model Lamb Wave Simulations	7
3.3	Influence of a Disbond Void on the Lamb Wave	8
4.	EXPERIMENTAL RESULTS AND DISCUSSION	10
4.1	Photoacoustic Technique to Measure the Dispersive Property	10
4.2	Influence of Ball Drop Impacts on Lamb Wave Test	11
4.3	Disbond Defects Induced by a Ball Drop	13
4.4	Relationship Between Lamb Wave Signal and Disbond Size	15
5.	SUMMARY AND CONCLUSIONS	16
6.	REFERENCES	17

LIST OF FIGURES

Figure		Page
1	Experimental System for Measuring the Dispersive Property of the GLARE Plate	2
2	The Lamb Wave Test Examination System	3
3	The Ball Drop Test	4
4	Thermal-Imaging Inspection System	5
5	Lamb Wave Dispersion Curves of GLARE 2A-2/1-0.4 for Phase Velocity and Group Velocity	6
6	The FEM for the Lamb Wave Simulations	7
7	Displacement Component of U_x and U_y Monitored at x = 200 mm on the top Surface of the GLARE Plate With Disbond Voids (x = 100 mm) of Various Sizes	9
8	Detected Lamb Wave Signals for Various Laser and PZT Distances and Phase Velocity of the GLARE Plate	11
9	Lamb Wave Testing at f = 695 kHz for Launching Signal and Detected Signal for Various Ball Impact Events	12
10	Detected A_0 Mode Lamb Wave Signal for Various Ball Impact Events and the Influence of the Impacts on the Detected A_0 Mode Lamb Wave Maximum Peak-to-Valley Voltages	13
11	Thermal Images of the Single-Sided Inspection of the Disbond Defect Area for 50, 100, 150, and 200 Impacts at 606 mJ	14
12	Disbond Defect Diameter Growth	15
13	Percentage of the Measured A_0 Mode Lamb Wave Voltage as a Function of the Disbond Diameter	16

LIST OF TABLES

Table		Page
1	Mechanical Properties of the 2024-T3 Alloy and S2/FM94 Glass Fiber-Reinforced Plastic Lamina	5
2	Amplitudes and Travel Times of the Displacement Component (U_y) of the A_0 Mode Lamb Wave Versus Void Sizes	10

LIST OF ACRONYMS

2D	Two-dimensional
Al	Aluminum
FEM	Finite element model
GLARE	GLAss-REinforced
NDE	Nondestructive evaluation
PVDF	Polyvinylidene fluoride
PZT	Lead zirconate titanate
RF	Radio frequency
SHM	Structural Health Monitoring

EXECUTIVE SUMMARY

The accelerated trend of replacing conventional materials with adhesively bonded polymer and polymer-metal composites in aircraft construction requires the development of structural health monitoring (SHM) systems that are appropriate to monitor the type of damage that the composite parts are likely to suffer. Structural degradation, whether engendered by inherent material aging due to the environment and service loads (fatigue, corrosion, etc.) or by unpredictable external events (impact, etc.), is an inevitable part of life. Intelligent SHM systems are needed to prevent structural failure of safety-critical structures such as aircraft that cannot be allowed to fail in service. The risk of unexpected failure could be dramatically reduced when the health-monitoring techniques are implemented. SHM systems aim to minimize the economic loss generated by unnecessary and premature replacement of expensive parts, without compromising safety. The goal of this project was to research the theoretical prediction and to demonstrate an integrated experimental diagnostic/prognostic system for monitoring impact damages in adhesively bonded composites.

This report describes a finite element model that simulates the influence of a disbond defect on the Lamb wave propagation in a GLAss-REinforced (GLARE) aluminum laminate. Both the displacement amplitudes and travel time of the A_0 mode Lamb wave were shown to be influenced by the disbond void. The calculation indicates that modally selected Lamb waves can be used to monitor the disbond growth.

The report presents the experimental results on a GLARE composite with a disbond defect induced by a series of ball drops. It was demonstrated that modally selective, guided Lamb waves were launched successfully and were used to detect the disbond defect in the GLARE plate. The measured A_0 mode Lamb wave signals were found to decay exponentially as the disbond diameter increases. It is shown that the disbond defect sizes can be predicted from the measured Lamb wave signals using the exponential model.

1. INTRODUCTION.

1.1 BACKGROUND.

GLAss-REinforced (GLARE) laminate is a class of fiber-metal laminates, consisting of thin, alternating bonded layers of metal sheets and fiber-reinforced epoxy prepreg [1]. The GLARE composites possess excellent properties from the combination of metals and fibrous composites [2]. As an example, the mechanical properties are enhanced by fiber bridging, which impedes crack propagation in the aluminum alloy layers when under cyclic tensile loading. For that reason, the GLARE composites offer outstanding fatigue resistance, excellent impact resistance, fire resistance, etc. [2]. The most attractive property is the weight reduction of at least 20% while exhibiting superior material properties, compared with the traditional aluminum alloy used in the aerospace industry [3]. Consequently, the GLARE composites are being used in a substantial part of the Airbus 380 fuselage [4 and 5].

1.2 PURPOSE.

There are many techniques for quantitative nondestructive evaluation (NDE) and structural health monitoring (SHM) of thin plate structures such as the GLARE composites. Guided Lamb wave techniques [6] have shown great potential for both NDE and SHM applications owing to their large area inspection capability [7]. Laser-generated ultrasonic waves have demonstrated many advantages to characterize the mechanical properties because of their noncontact, nondestructive, and broadband nature [8]. While laser ultrasonics can be a good NDE tool for off-line inspection, it is not a viable candidate for online SHM of the growth of disbond defects when predicting the remaining life of the GLARE composite. For SHM applications, a modally selective piezoelectric sensor is a versatile tool [9 and 10]. One objective of this work was to theoretically study the A_0 mode Lamb wave interaction with a disbond void in a GLARE plate to develop an appropriate modally selective SHM sensor to monitor disbond growth.

Structural degradation, whether engendered by inherent material aging due to the environment and service loads (fatigue, corrosion, etc.) or by unpredictable external events (impact, etc.), is inevitable. Intelligent SHM systems are required to predict structural failure of safety-critical structures, such as airplanes, which are not allowed to fail in service. For the application of adhesively bonded composites, disbond defects are a matter of serious concern in safety-critical aerospace composite parts in service [11]. In the past, ball drop-induced delamination in the GLARE composites was reported and correlated to various factors, including impact energy [11 and 12], impact events [12 and 13], and material post-curing effect [13]. To monitor the impact damages in adhesively bonded composites, the assessment of the influence of the disbond defect on the Lamb wave propagation is significant, especially in designing appropriate sensors for SHM of these composite structures.

1.3 REPORT OVERVIEW.

In this report, the effect of the disbond defects on the Lamb wave propagation in a GLARE plate will be explored theoretically and experimentally. The theoretical investigation was conducted with a finite element model (FEM). A series of experiments were introduced on photoacoustic

techniques, guided Lamb wave generation and detection, ball drop-induced disbond defects, and thermal-imaging techniques. The relationship between the disbond defect size and the detected Lamb wave amplitudes were ascertained from the experimental results. It was demonstrated that modally selective Lamb waves can be effectively used to detect impact damage and estimate disbond defect size in the GLARE composite.

2. EXPERIMENTS.

GLARE 2A-2/1-0.4 was selected for the experimental tests. The GLARE plate consisted of two layers of aluminum alloy (0.4 mm thick) and one layer of glass fiber/epoxy prepreg (0.25 mm thick), forming a sandwich structure. The prepreg orientation in each fiber layer was 0/0. The GLARE plate was purchased from Fibre Metal Laminates Center of Competence in the Netherlands, where the GLARE composites were invented.

2.1 PHOTOACOUSTIC TECHNIQUE.

The dispersive property of the GLARE plate was measured with a photoacoustic technique. As shown in figure 1, an experimental system was built to measure the dispersive property of the sample. A pulsed laser (wavelength = 1064 nm, pulse width = 8 ns, power = 167 mJ/pulse) was focused with a cylindrical lens to a line source. The absorbed energy from the laser was transformed into kinetic energy, resulting in Lamb waves in the sample. A small lead zirconate titanate (PZT) transducer was mounted on the GLARE plate with conductive epoxy. The propagating Lamb waves were detected with the PZT receiver and were monitored and recorded with a digital oscilloscope. A photoelectric diode was used as a trigger signal for the oscilloscope. The distance between the laser and the PZT receiver was varied from 75 mm to 125 mm.

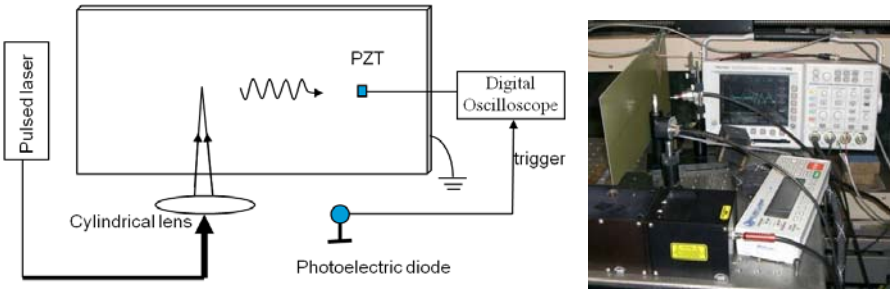

(a) (b)

Figure 1. Experimental System for Measuring the Dispersive Property of the GLARE Plate
(a) Schematic and (b) Test Setup

2.2 LAMB WAVE TEST.

Polyvinylidene fluoride (PVDF) film, provided by Measurement Specialties, Inc., was used as the piezoelectric media for the Lamb wave transducers. The PVDF film is thin (110 μm) and flexible, which produces low-profile and low-cost malleable sensors. The PVDF film was attached to the GLARE plate with M-Bond 200 and copper comb electrodes were mounted directly to the PVDF film. Both the transmitter and the receiver have the same electrode

configurations. Each transducer has 10 electrode fingers with a 20-mm finger length and 2.45-mm spacing between fingers. One transducer was used to launch Lamb waves and the other detected the signals from the other side of the plate. The distance between the inner edges of the two PVDF transducers was 200 mm.

Figure 2 shows the Lamb wave test examination system. Ten cycles of a Hanning-windowed tone-burst signal were generated from a function generator with the form of

$$V(t)\begin{cases}\frac{V_0}{2}\left[1-\cos(2\pi f_0 t / n_0)\right]\cos(2\pi f_0 t), & t \le n_0 / f_0 \\ 0, & t > n_0 / f_0\end{cases} \tag{1}$$

where V_0 = 250 mV is the peak-to-peak voltage, f_0 = 695 kHz is the central frequency, and n_0 = 10 is the number of the sinusoidal cycles within the Hanning window. The excitation signal was amplified by a radio frequency (RF) amplifier (gain of 377) before applying it to the electrodes of the PVDF transmitter and generating Lamb waves in the GLARE plate. The Lamb wave signals were picked up by the PVDF receiver and a signal conditioner was applied before being recorded by a digital oscilloscope. An active three-pole low-pass filter was built to filter out noise and suppress undesired modes of Lamb wave signals. The cut-off frequency of the filter was set to ~1 MHz with a roll-off slope of -60 dB/decade. The filtered Lamb wave signals were amplified by a pre-amp with a gain of 34 dB.

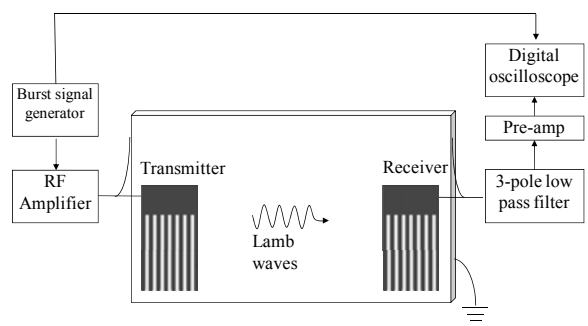

(a)

(b)

Figure 2. The Lamb Wave Test Examination System (a) Schematic and (b) Experimental Setup

2.3 BALL DROP TEST.

A ball drop test was used to introduce disbond defects in the GLARE plate. As shown in figure 3, the ball drop test was performed by releasing a 1-inch-diameter steel ball from a height of 3 feet to strike the center point of the GLARE plate between the two PVDF comb transducers. The impact energy was 606 mJ converted from the kinetic energy of the falling ball. The number of impact events ranged from 0 to 200 times. After each ball drop test, the experimental Lamb wave measurement system was used to study the influence of ball drops on the detected Lamb wave signals.

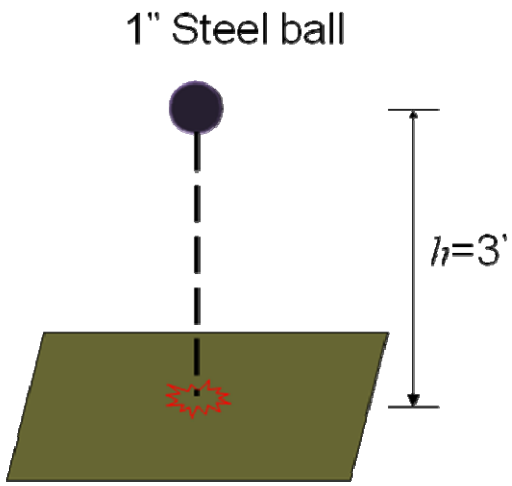

Figure 3. The Ball Drop Test

2.4 THERMAL-IMAGING TECHNIQUE.

After each ball drop test, the GLARE plate was examined with a thermal-imaging system, FLIR ThermoVision SC6000, by single-sided inspection. Figure 4 shows the thermal-imaging inspection system. Two flash lamps were used to irradiate the sample surface to generate a temperature gradient in the GLARE plate. Thermal images were taken in time sequence, starting just before the pulsed light irradiation and ending some time after to include temperature-dependent phenomena. The camera was equipped with a linear Stirling-cooled focal plane array indium antimonide detector working in the medium-wave infrared band at 3-5 μm. The acquisition rate was 50 Hz with a full frame size of 640 by 512 pixels. A thin layer of washable black paint was applied on the GLARE sample surface to enhance the light absorption.

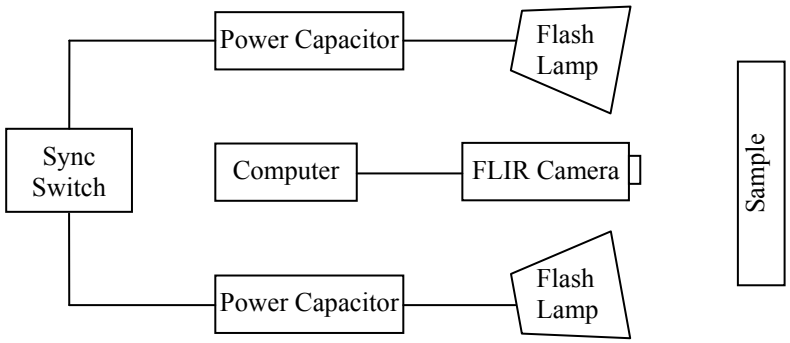

(a)

(b)

Figure 4. Thermal-Imaging Inspection System (a) Schematic and (b) Experimental Setup

3. THEORY.

3.1 DISPERSIVE PROPERTY OF THE GLARE PLATE.

The component materials used to fabricate the GLARE plate were aluminum (Al) 2024-T3 supplied by Austria Metal AG and Alcan Singen GMGH, and Prepreg FM94 (67% S2 glass) provided by Cytec Industries, Inc. The mechanical properties for each layer are summarized in table 1.

Table 1. Mechanical Properties of the 2024-T3 Alloy and S2/FM94 Glass Fiber-Reinforced Plastic Lamina

Layer	Density (kg/m^3)	Elastic Modulus E_{11} (GPa)	Poisson's Ratio υ	Thickness (mm)
2024-T3 Al alloy [14]	2780	73.1	0.33	0.40
S2/FM94 [15]	1980	52.0	0.25	0.25

Based on the above nominal values of the mechanical properties for each layer, the Lamb wave dispersion curves of this specimen were calculated numerically by using the classical transfer matrix method for layered media [16]. Figure 5(a) shows the theoretical phase velocity dispersion curves of the GLARE plate. As shown in figure 5(b), the group velocity dispersion curves were calculated from the phase velocity of the GLARE composite using:

$$V_g = V_p - \lambda\,(dV_p/d\lambda) \tag{2}$$

where V_g is the group velocity, V_p is the phase velocity, and λ is the wavelength of the Lamb waves.

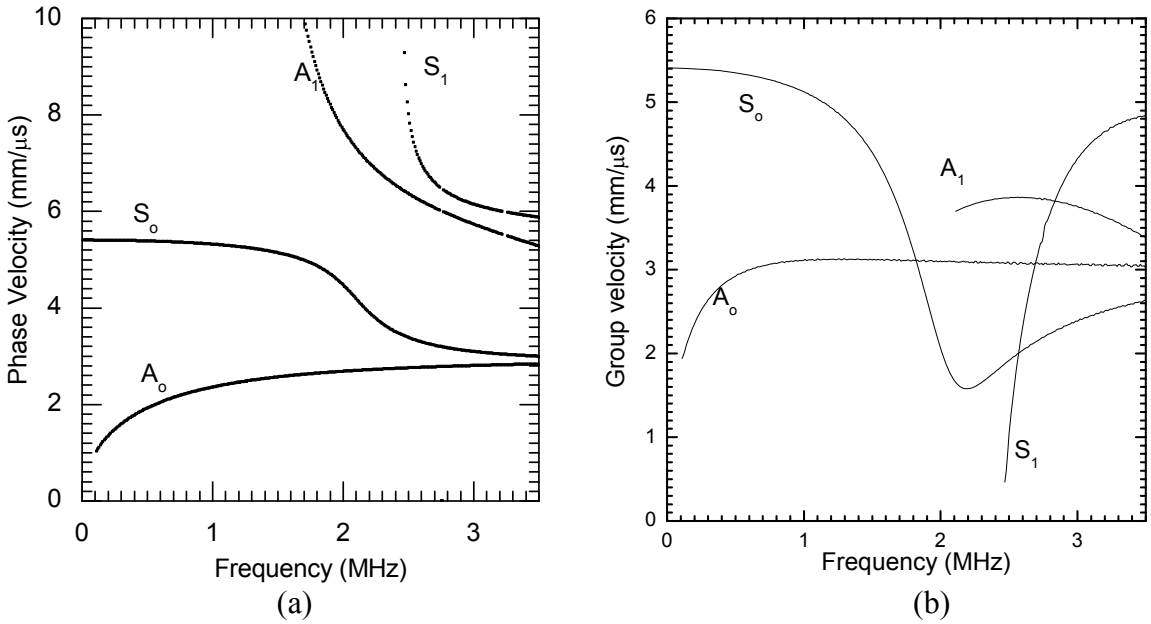

Figure 5. Lamb Wave Dispersion Curves of GLARE 2A-2/1-0.4 for (a) Phase Velocity and (b) Group Velocity

As shown in figure 5, Lamb waves are multimodal and highly dispersive. It is important to select a proper frequency to use Lamb waves for disbond detection. Three factors need to be considered for an appropriate selection of the driving frequency. First, the driving frequency should be high enough so that the wavelength of the Lamb wave is comparable to the scale of local disbonds [17 and 18]. Second, the input frequency also needs to be low so that higher-order modes do not clutter the fundamental symmetric (S_0) and anti-symmetric (A_0) modes. Third, it is helpful to select the frequency in a relatively flat region from the dispersion curves, which makes the subsequent signal processing for disbond detection easier and repeatable. Therefore, A_0 mode with an input frequency of 950 kHz was selected for the modeling. Note that the A_0 mode wavelength is smaller than the S_0 mode at the desired frequency, which makes it more sensitive to the disbond defects. The corresponding wavelengths are 2.45 and 5.61 mm for A_0 mode and S_0 mode, respectively.

3.2 FINITE ELEMENT MODEL LAMB WAVE SIMULATIONS.

As indicated in reference 10, modally selective transducers can be used effectively as SHM tools to monitor the size of disbonds. To investigate the design parameters for such sensors, an FEM was constructed to investigate the influence of disbonds on the Lamb wave propagation in the GLARE plate. Computations were made with the commercial software ANSYS®. As shown in figure 6, Lamb waves were launched with a PVDF film by applying tone-burst voltages on the piezoelectric film with a 10-finger comb pattern. The layer thicknesses of the GLARE plate were based on the product dimensions shown in table 1. The PVDF film thickness was 110 µm, which is the typical thickness available from commercial vendors. The length of the GLARE plate in the FEM model was 400 mm. The spacing of the tone-burst voltage was 2.45 mm, which matched the wavelength of the A_0 mode Lamb wave. There were at least 20 nodes per wavelength and a full transient analysis was done with the integration time steps of ~1-4×10^{-8} s. The selected time step satisfies the optimum value of less than the travel time of Lamb waves in an element size for the studied frequency. Plane 13 (two-dimensional (2D) structural solid) and Plane 42 (2D coupled-field solid) were selected as elements for the PVDF film and the GLARE plate, respectively.

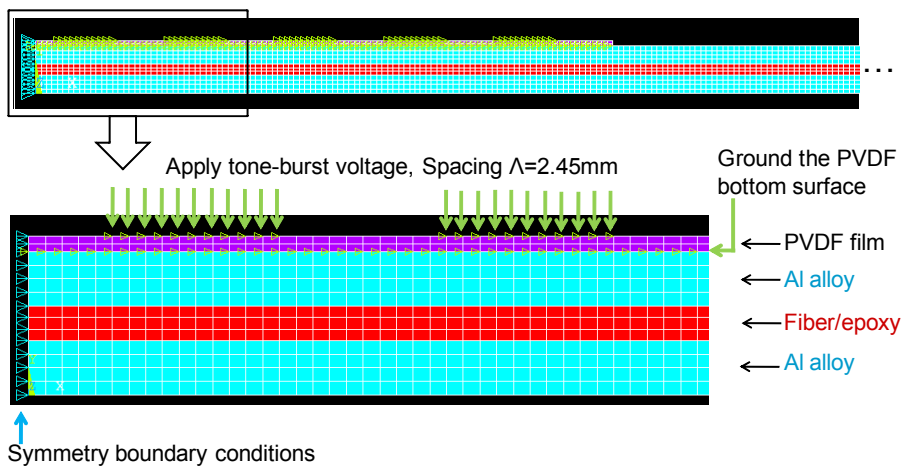

Figure 6. The FEM for the Lamb Wave Simulations

To launch narrow-band Lamb waves in the GLARE plate, the excitation sinusoidal signal with Hanning window (equation 1) was applied on the top surface of the PVDF film. In this FEM model, V_o = 400 Volts, f_o = 950 kHz, and n_o = 5. Only half the plate was modeled by applying a symmetry boundary condition for the x-displacement, U_x, at x = 0. The bottom surface of the PVDF film was electrically grounded by applying 0 Volts to the nodes at the interface between the PVDF film and the Al alloy layer.

The influence of a disbond on the Lamb wave propagation was studied by creating a void in the fiber/epoxy layer. The disbond void was located at x = 100 mm. The length of the disbond varied from 0.1-4.0 mm while keeping a constant height of 0.25 mm, which was the thickness of the fiber/epoxy layer. The displacement of the propagated Lamb wave was monitored on the top surface of the GLARE plate at x = 200 mm.

3.3 INFLUENCE OF A DISBOND VOID ON THE LAMB WAVE.

Figure 7 shows the displacement components, U_x and U_y, on the top surface of the GLARE plate at x = 200 mm for various void sizes at x = 100 mm. The black curves show the Lamb wave propagation for the GLARE plate without a disbond void. As observed, the A_0 mode Lamb wave was successfully launched with the PVDF comb transducer in the FEM, and the propagation of Lamb waves is clearly indicated. The S_0 mode Lamb wave with much smaller amplitudes was also present in the FEM model, as shown in figure 7, which is inevitable for the narrow-band launching signal and the limited width of the comb transducer in the FEM simulations.

As shown in figure 7, the effect of four different disbond sizes (given in length by height of the disbond void) was compared to the Lamb wave propagation in the GLARE plate: 0.5 by 0.25 mm (green), 1.0 by 0.25 mm (blue), 2.0 by 0.25 mm (pink), and 4.0 by 0.25 mm (gray). The displacement component amplitudes for the A_0 mode Lamb wave decreased as the disbond length increased from 0.5 to 1.0 mm. However, this trend changed when the void length was larger than 1.0 mm. The smaller displacement amplitudes in the A_0 mode Lamb wave are attributed to the reflection and scattering of the Lamb wave by the disbond. Figure 7 also shows an oscillation tail in the Lamb wave displacements for the 2.0- by 0.25-mm voids. Void sizes can result in an oscillation tail in the A_0 mode Lamb wave displacements. The oscillation tail can be attributed to the multiple reflections of Lamb waves in the void region, and thus, the disbond void behaves like a "resonator," generating exponential decayed Lamb waves.

In addition to the influence on the displacement amplitudes, there is a time delay for the A_0 mode Lamb wave propagating through the disbond void of various sizes. As the Lamb wave reaches the disbond area where the void separates the GLARE plate into two symmetric sections (Al alloy layers) with less than half of the whole plate thickness, the Lamb wave is forced to propagate through the two adjoining sections. The lower phase velocity of the A_0 mode Lamb wave propagating in the disbond region results in the time delay at the monitored spot. Therefore, the A_0 mode Lamb wave travel time increased as the void length increased. Both the influence of the disbond void on the displacement amplitudes and the travel time of the A_0 mode Lamb wave can be clearly observed in the figure 7 insets. This is consistent with the results of Petculescu, et al. [10], and indicates that time-delay measurements can serve as a basis for developing SHM sensors for online monitoring of disbond growth.

As an example, the quantitative influence of a disbond void on the A_0 mode Lamb wave (U_y component) is summarized in table 2. There is a negligible effect on the Lamb wave displacement when the disbond void size is 0.1 by 0.25 mm. The influence is less than 1% on the reduced displacement amplitudes. However, the influence of the disbond void becomes significantly more important in determining the A_0 mode Lamb wave amplitudes as its size increases. For instance, the percentage of the reduced displacement amplitudes reaches ~47% as the void length increases to 1.0 mm.

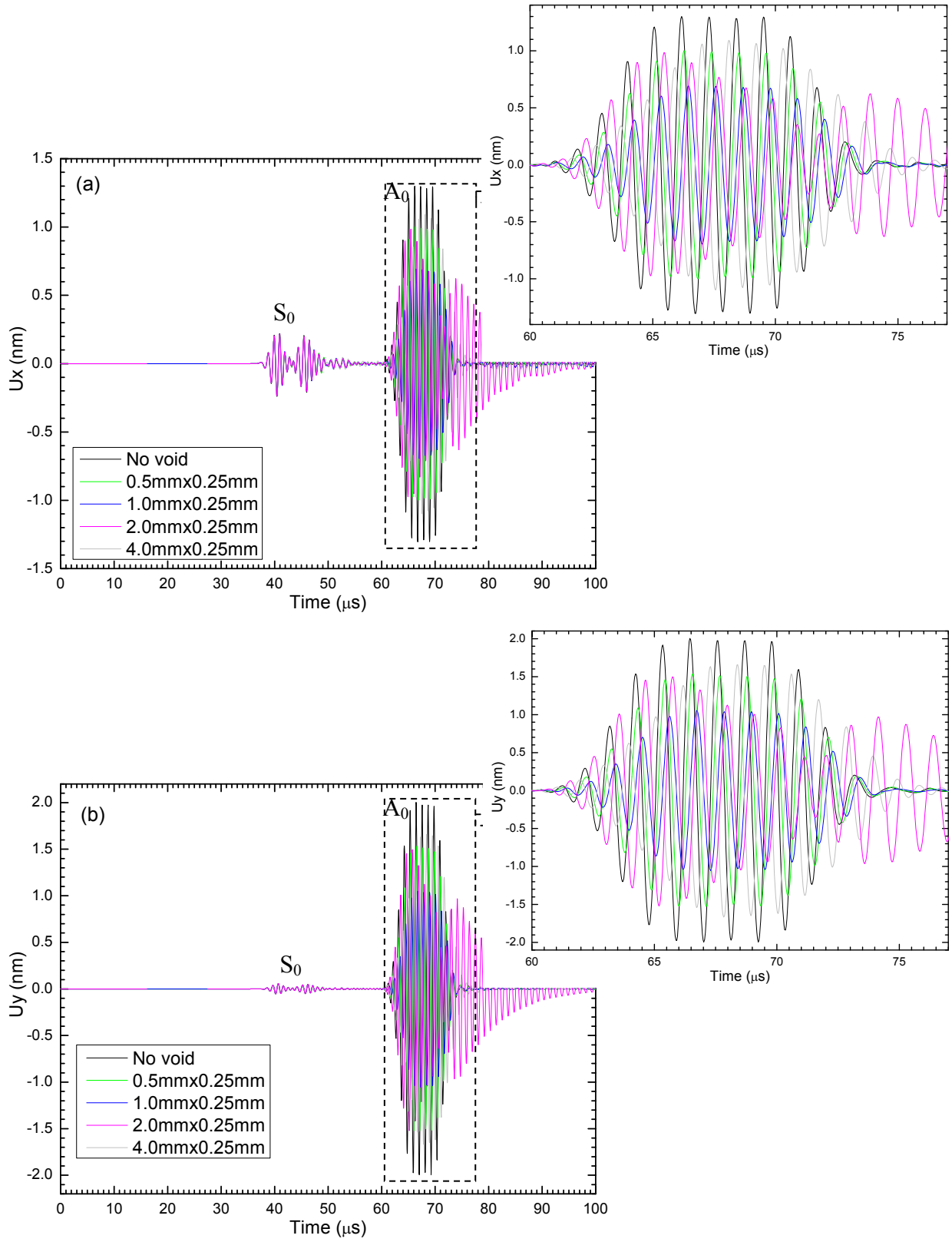

Figure 7. Displacement Component of (a) U_x and (b) U_y Monitored at x = 200 mm on the top Surface of the GLARE Plate With Disbond Voids (x = 100 mm) of Various Sizes

Table 2. Amplitudes and Travel Times of the Displacement Component (U_y) of the A_0 Mode Lamb Wave Versus Void Sizes

Void Length (mm)	Void Height (mm)	U_y Maximum Amplitude (nm)	Percentage of U_y Maximum Amplitude (%)	Arrival Time of the First U_y Peak (ms)	Time Delay in U_y (ms)
0	0	2.00	--	61.23	--
0.1	0.25	1.99	99.5	61.23	0
0.5	0.25	1.53	76.5	61.29	0.06
1.0	0.25	1.05	52.5	61.44	0.21
2.0	0.25	1.50	75.0	61.56	0.33
4.0	0.25	1.65	82.5	61.98	0.75

The travel time of the first peak of the A_0 mode Lamb waves (U_y component) was traced for the GLARE plate with and without any disbond voids, as shown in table 2. There is no measurable time delay when the disbond void size is less than or equal to 0.1 by 0.25 mm. However, the time delay increases from 0.06 to 0.75 μs when the disbond lengths increase from 0.5 to 4.0 mm. These results imply that the A_0 mode Lamb wave signal is very sensitive to the disbond void and can be used for the SHM of adhesively bonded composites. The resolution of the disbond detection can be as small as 0.1 mm with the A_0 mode Lamb wave at the selected frequency.

4. EXPERIMENTAL RESULTS AND DISCUSSION.

4.1 PHOTOACOUSTIC TECHNIQUE TO MEASURE THE DISPERSIVE PROPERTY.

The dispersive property of the GLARE plate was first measured with the experimental setup shown in figure 1. Lamb wave signals were recorded for various combinations of laser and PZT distances, as shown in figure 8(a). The frequencies launched with the current setup are around 0.2-1.3 MHz. The first Lamb wave signals correspond to the S_0 mode, which indicates faster velocities for the lower-frequency signal. The second group of signals is a reflection from the sample edge for the S_0 mode Lamb waves. The A_0 mode signals arrive even later because they have lower speeds. In addition, the A_0 mode is highly dispersive at low-frequency range, and the phase velocities increase with increasing frequencies.

The measured Lamb wave signals were used to calculate the phase velocity by phase unwrapping using:

$$c(f) = \frac{2\pi f \cdot \Delta d}{\Delta\Phi(f)} \tag{3}$$

where, f, Δd, and $\Delta\Phi$ are frequency, distance, and phase difference, respectively. As indicated in figure 8(b), the measured phase velocities are consistent with the theoretical predications. However, figure 8(b) only shows part of the measured phase velocity for A_0 mode because of

interference from unwanted signals from the boundary reflection. Overall, the measured dispersive properties confirm the theoretical calculations from the mechanical properties of the GLARE plate in table 1.

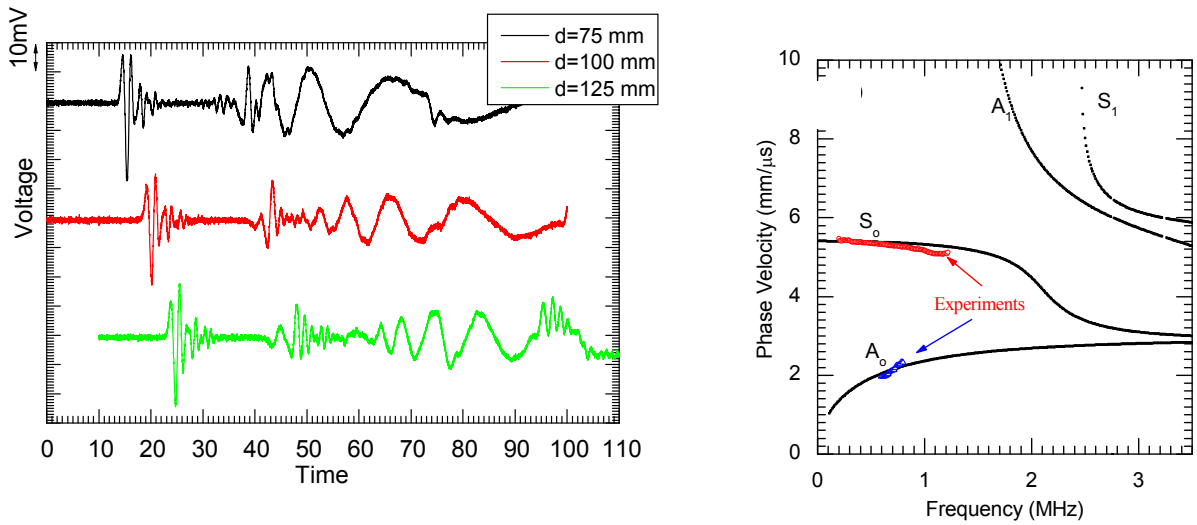

(a) (b)

Figure 8. (a) Detected Lamb Wave Signals for Various Laser and PZT Distances and (b) Phase Velocity of the GLARE Plate (Solid curves for the theoretical calculations; open circles and triangles for the experimental measurements)

4.2 INFLUENCE OF BALL DROP IMPACTS ON LAMB WAVE TEST.

As shown in figure 9, guided Lamb waves were demonstrated to be launched successfully and were used to study the influence of the disbond defect on the A_0 mode Lamb wave signals at a frequency of 695 kHz. Figure 9(a) shows the launching signal of ten cycles of the tone-burst waveform generated with a function generator. The black curve in figure 9(b) is the detected signal for the pristine condition of the GLARE. The traveling time for the first cycle of A_0 mode Lamb wave is t = 88.3 μs. The distance between the two PVDF comb transducers is d = 200 mm. The phase velocity is calculated to be V_p = 2.265 mm/μs. As a result, the obtained phase velocity is close to the theoretical expectation of 2.143 mm/μs at a frequency of 695 kHz. The discrepancy on the phase velocity may be due to the deviation of the material properties from the theoretical calculations.

The signals at the very beginning of figure 9(b) are the electrical coupling from the emission of the excitation source. It is also notable that there is a group of weak signals between 40 and 60 μs. The first part of this group appears to be the S_0 mode since its velocity is estimated to be close to the theoretical expectation. The second part of this group has a frequency of ~2.2 MHz, which is about three times the launching signal frequency. These are likely to be from the A_1 or S_1 modes, although they are not intended to be launched by the transducer. Figure 9(b) also shows the detected Lamb wave signals collected for various ball impact events of 20~200 times.

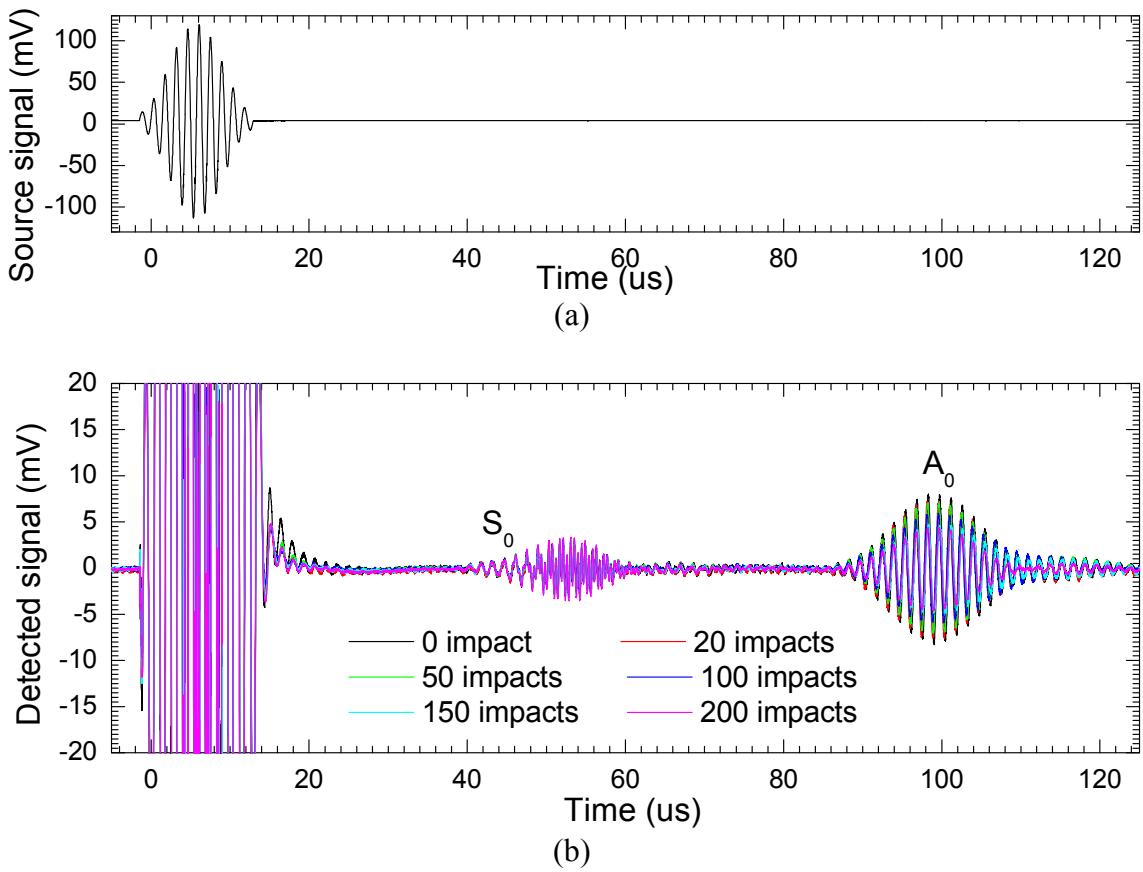

Figure 9. Lamb Wave Testing at f = 695 kHz for (a) Launching Signal and (b) Detected Signal for Various Ball Impact Events

Figure 10(a) shows the detected A_0 mode Lamb wave signals for various ball impacts. As shown, the measured A_0 mode Lamb wave signals decrease as the ball impact events increase. The maximum peak-to-valley voltages of the detected A_0 mode Lamb waves can be obtained for various impact numbers, which are plotted in figure 10(b). A linear fit was used to fit the experimental data with the least square method. The linear relationship between the detected A_0 mode Lamb wave amplitudes and the number of impacts is indicated from the good correlation coefficient (R = -0.984). The closer the coefficient is to -1, the stronger the correlation between the experimental data and the fitting line.

It is notable that the detected A_0 mode Lamb waves arrive almost at the same time for various impact events. There is no apparent time delay or a consistent trend on the travel time of the selected A_0 mode Lamb wave as the number of impacts increases. In previous research, Petculescu, et al., reported that time delay grows steadily as the impact damage accumulates on a carbon-epoxy, cross-ply composite panel [10]. They attributed the time delay to the lower effective material stiffness induced by the continuous impacts, which results in a lower velocity and therefore an increase in time delay. The discrepancy between the two experimental results could be attributed to the different composite material structures.

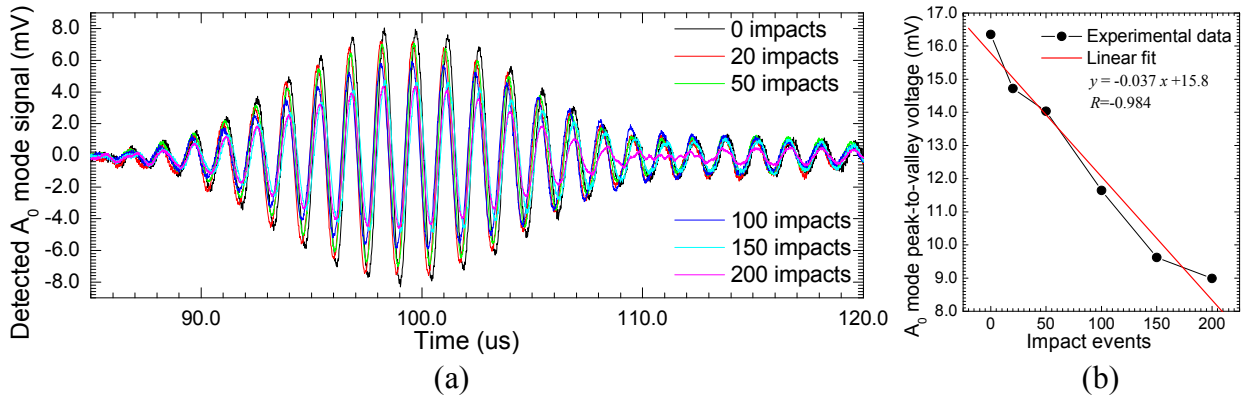

Figure 10. (a) Detected A_0 Mode Lamb Wave Signal for Various Ball Impact Events and (b) the Influence of the Impacts on the Detected A_0 Mode Lamb Wave Maximum Peak-to-Valley Voltages

In the previous section, theoretical calculations predicted that both the displacement amplitudes and travel time of the A_0 mode Lamb wave were shown to be influenced by a disbond void. The travel time of the A_0 mode Lamb wave increases as the disbond size increases. The experiments, however, show no trace of consistent time delay tested in the GLARE composite. The discrepancy between the theory and the experiment could be due to the fact that the disbond defect sizes (<8 mm) are not large enough compared to the transducer electrode comb length (20 mm), and thus, Lamb waves could bypass the disbond area without being affected. In addition, the modeled "disbond void" cannot represent the actual disbond defect perfectly. The ball impact involves not only delaminations at the interfaces, but also damage of the glass fiber and matrix. The reduced amplitude with the ball impact could be caused by the disbond between the transducers and the GLARE plate. However, this possibility can be excluded by observing the detected signals between 40 and 60 µs in figure 9. The amplitudes of this portion of signals are actually enhanced, instead of reduced, as the number of impacts increases. The most likely change in amplitude is therefore mode conversion from the A_0 mode to higher modes.

4.3 DISBOND DEFECTS INDUCED BY A BALL DROP.

The disbond defect was further confirmed and measured with a thermal-imaging system. An active thermal-imaging technique was achieved by applying an external light heat source to stimulate heat flow within the GLARE plate. The surface was monitored for spatial temperature variations as it returned to thermal equilibrium. As an example, figure 11 shows the thermal images of the disbond defect area for (a) 50, (b) 100, (c) 150, and (d) 200 impacts. These images were captured 0.02 second after triggering the flash lamps. The black areas are the undamaged GLARE plate and the white spots in the center are the induced disbond defects. The smaller thermal conductivity and its discontinuity around the disbond defect region led to a higher temperature on the corresponding monitored surface. Therefore, the "hot" area (white in the thermal images) represents the disbond defect in the glass fiber epoxy layer. These spatial variations can be an indication of internal flaws, such as disbond defects, that tend to increase the thermal impedance of the structure. The enhanced thermal impedance due to the disbond defect can result in localized surface temperature differentials up to a few tens of Kelvins. Note that although there were some traces left on the black area, which are caused by the nonuniform ink

painting, the overall information about the disbond defect can still be clearly acquired for the size measurement.

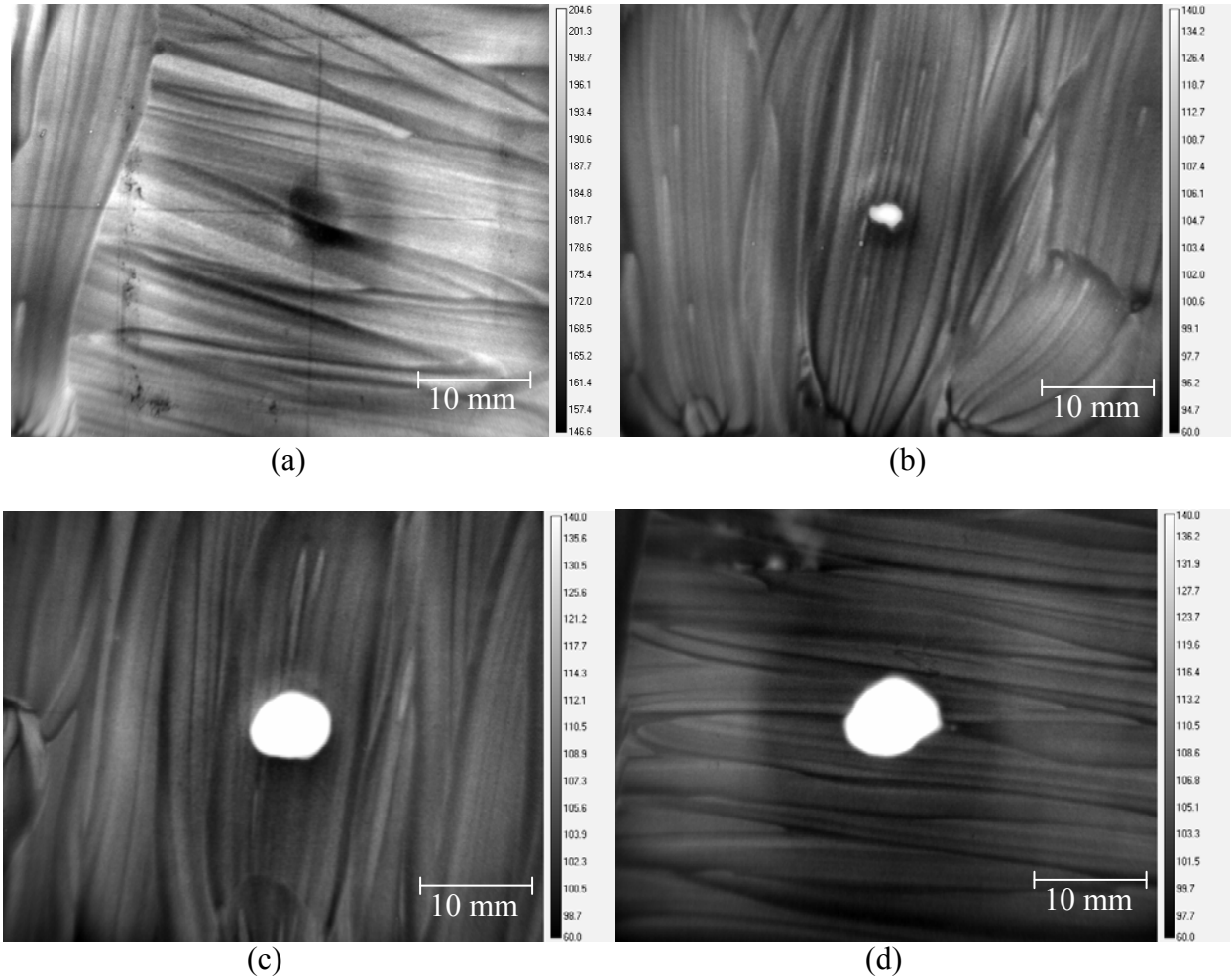

Figure 11. Thermal Images of the Single-Sided Inspection of the Disbond Defect Area for (a) 50, (b) 100, (c) 150, and (d) 200 Impacts at 606 mJ

As shown in figure 12, the size of the disbond defect was measured by comparing the thermal image pixels and the ruler on the GLARE plate surface. As expected, the disbond defect diameter increased as the number of impacts increased. It is notable that the disbond defects of 50 or less ball impacts was not detectable with the thermal-imaging system. When comparing the sensitivity to disbond defects, the A_0 mode Lamb wave amplitude is more sensitive to the ball impacts. As shown in figure 10(b), the Lamb wave detection shows a 10.0% decrease in A_0 mode amplitude after 20 impacts. Therefore, Lamb wave examination has proven to be efficient on disbond defects, especially for the in situ SHM application.

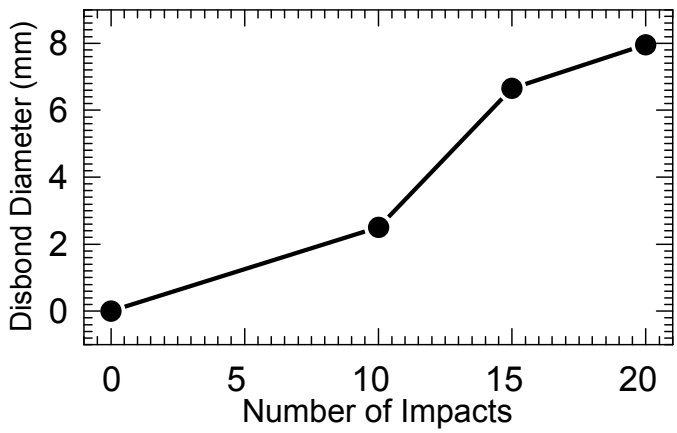

Figure 12. Disbond Defect Diameter Growth

4.4 RELATIONSHIP BETWEEN LAMB WAVE SIGNAL AND DISBOND SIZE.

Figure 13 shows the measured A_0 mode Lamb wave signal reduced with increased disbond defect diameter. The reduced A_0 mode Lamb wave amplitudes can be attributed to wave reflection [19], scattering [20], and mode conversion in the disbond defect area. The mode conversion in the disbond defect region can be further confirmed from the collected signals between 40 to 60 μs shown in figure 9. The amplitudes in this time interval increased as the number of impacts increased. A first-order exponential decay was used to fit the percentage of the measured A_0 mode Lamb wave voltage versus the disbond defect diameter. The equation can be expressed as

$$y = \exp(-x / D_0) \tag{4}$$

where y is the percentage of the measured A_0 mode Lamb wave voltage and x is the disbond defect diameter. The best least square fit is D_0 = 12.0 ±1.5 mm with a good correlation coefficient of R^2 = 0.91. The fitting parameter D_0 represents the sensitivity of the Lamb wave detection system. The smaller the D_0 is, the more sensitive the Lamb wave detection system is for the small disbond defect. On the other hand, a larger D_0 value means the Lamb wave detection system can be effectively used to monitor a bigger disbond defect. The parameter D_0 is believed to rely on the structure of the GLARE composite as well as the configuration of the disbond defect and the Lamb wave transducers. Further research is needed to clarify the influence of these factors on the parameter D_0 as this is of critical significance to the application of the Lamb wave in the SHM of the disbond defects.

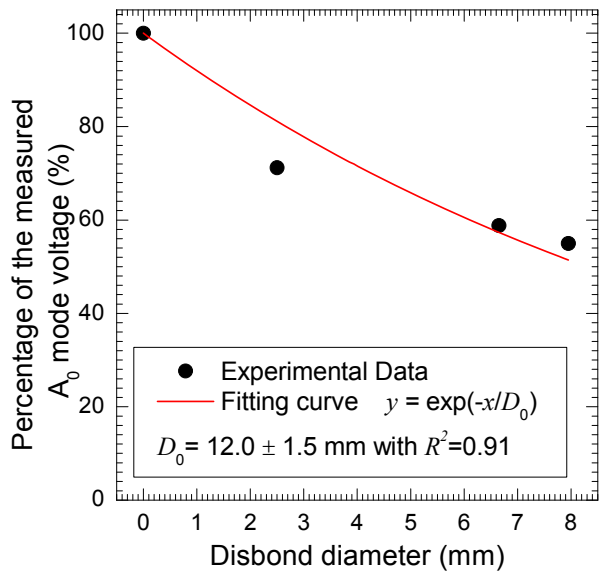

Figure 13. Percentage of the Measured A_0 Mode Lamb Wave Voltage as a Function of the Disbond Diameter

5. SUMMARY AND CONCLUSIONS.

A finite element model was built to simulate the influence of a disbond on the Lamb wave propagation. Both the displacement amplitudes and travel time of the A_0 mode Lamb wave were shown to be influenced by the disbond void. For a void length less than 1 mm, the displacement amplitudes reduced as the void size increased. This trend was not valid for a void length larger than 1.0 mm. The time delay increased as the disbond sizes increased, which can be used as the parameter to monitor a disbond defect growth in the GLAss-REinforced (GLARE) plate. From the calculated result at the selected frequency, the detectable disbond void size can be predicted to be as small as 0.1 mm.

In experiments, Lamb waves launched with a pulsed laser were used to measure the dispersive properties of the GLARE plate. The experimental measured dispersion curves were consistent with the theoretical calculations. A series of ball drops was used to introduce a disbond defect in the GLARE plate. The disbond defect was confirmed and measured with a thermal-imaging system. Modally selective, guided Lamb waves were demonstrated to be launched successfully and were used to detect the disbond defect in the GLARE plate. The measured A_0 mode Lamb wave signals decreased linearly as a function of the ball impact events. By combining the thermal-imaging results, the collected A_0 mode Lamb wave signals were found to decay exponentially as the disbond diameter increased. It was shown that the disbond defect sizes can be predicted from the measured Lamb wave signals using a simple exponential model.

Because of the properties of GLARE, very small disbonds caused from drop weight impacts like those in this study are not likely to have a significant affect on the residual strength. Therefore, there may be no need to find such small disbonds in real GLARE structures. This may be important for future work and subsequent steps of development where realistic structural details affect wave propagation making it more difficult to detect small disbonds.

6. REFERENCES.

1. Rosalie, S.C., Vaughan, M., Bremner, A., and Chiu, W.K., "Variation in the Group Velocity of Lamb Waves as a Tool for the Detection of Delamination in Glare Aluminum Plate-Like Structures," *Composite Structures,* Vol. 66, Nos. 1-4, 2004, pp. 77-86.

2. Wu, G.C. and Yang, J.M., "The Mechanical Behavior of Glare Laminates for Aircraft Structures," *Journal of the Minerals, Metals & Materials Society,* Vol. 57, No. 1, 2005, pp. 72-79.

3. Botelho, E.C., Silva, R.A., Pardini, L.C., and Rezende, M.C., "A Review on the Development and Properties of Continuous Fiber/Epoxy/Aluminum Hybrid Composites for Aircraft Structures," *Materials Research*, Vol. 9, 2006, pp. 247-256.

4. Vermeeren, C., "An Historic Overview of the Development of Fibre Metal Laminates," *Applied Composite Materials,* Vol. 10, Nos. 4-5, 2003, pp. 189-205.

5. Vlot, A., "*Glare History of the Development of a New Aircraft Material*," Kluwer Academic Publishers, Dordrecht, The Netherlands, 2001.

6. Kirikera, G.R., Sun, L., Kil, H.G., Krishnaswamy, S., and Achenbach, J.D., "Matched Ultrasonic Transducers and Assessment of Transducer Performance for Robust Structural Health Monitoring Applications," *Review of Progress in Quantitative Nondestructive Evaluation*, 2008, pp. 1436-1444.

7. Liu, T., Veidt, M., and Kitipornchai, S., "Single Mode Lamb Waves in Composite Laminated Plates Generated by Piezoelectric Transducers," *Composite Structures,* Vol. 58, No. 3, 2002, pp. 381-396.

8. Scudder, L.P., Hutchins, D.A., and Guo, N.Q., "Laser-Generated Ultrasonic Guided Waves in Fiber-Reinforced Plates—Theory and Experiment," *IEEE Transactions on Ultrasonics Ferroelectrics and Frequency Control*, Vol. 43, No. 5, 1996, pp. 870-880.

9. Demcenko, A., Zukauskas, E., Kazys, R., and Voleisis, A., "Investigation of Interaction of the Lamb Wave With Delamination Type Defect in Glare Composite Using Air-Coupled Ultrasonic Technique," *Proceeding of Forum Acusticum (Budapest)*, 2005, pp. 2817-2822.

10. Petculescu, G., Krishnaswamy, S., and Achenbach, J.D., "Group Delay Measurements Using Modally Selective Lamb Wave Transducers for Detection and Sizing of Delaminations in Composites," *Smart Materials & Structures*, Vol. 17, No. 1, 2008, pp. 015007.

11. Vijay Kumar, R.L., Jawali, N.D., Srikanth, L., Rahul Kumar, C., Prakash, M.R., and Rao, R.M.V.G.K., "Post Impact Compression Strength (PICS) Evaluation of Glass/Epoxy Composite Using a Novel Approach—Effect of Delamination Area," *Journal of Reinforced Plastics and Composites*, Vol. 26, No. 11, 2007, pp. 1101-1109.

12. Bagnoli, F., Bernabei, M., Figueroa-Gordon, D., and Irving, P.E., "The Response of Aluminium/Glare Hybrid Materials to Impact and to In-Plane Fatigue," *Materials Science and Engineering A-Structural Materials Properties Microstructure and Processing,* Vol. 523, Nos. 1-2, 2009, pp. 118-124.

13. Kumar, C.R., Radhakrishna, K., and Rao, R.M.V.G.K., "Postcuring Effects on Impact Behavior of Glass/Epoxy Composite Laminates," *Journal of Reinforced Plastics and Composites,* Vol. 24, No. 9, 2005, pp. 949-960.

14. "ASM Material Data Sheet: Aluminum 2024-T3," Aerospace Specification Materials Inc.

15. Fatt, M.S.H., Lin, C.F., Revilock, D.M., and Hopkins, D.A., "Ballistic Impact of GLARE™ Fiber-Metal Laminates," *Composite Structures*, Vol. 61, Nos. 1-2, 2003, pp. 73-88.

16. Cheng, A., Murray, T.W., and Achenbach, J.D., "Simulation of Laser-Generated Ultrasonic Waves in Layered Plates," *Journal of the Acoustical Society of America,* Vol. 110, No. 2, 2001, pp. 848-855.

17. Sohn, H., Park, G., Wait, J.R., Limback, N.P., and Farrar, C.R., "Wavelet-Based Active Sensing for Delamination Detection in Composite Structures," *Smart Materials & Structures*, Vol. 13, No. 1, 2004, pp. 153-160.

18. Sohn, H., Park, H.W., Law, K.H., and Farrar, C.R., "Damage Detection in Composite Plates by Using an Enhanced Time Reversal Method," *Journal of Aerospace Engineering*, Vol. 20, No. 3, 2007, pp. 141-151.

19. Hu, N., Shimomukai, T., Yan, C., and Fukunaga, H., "Identification of Delamination Position in Cross-Ply Laminated Composite Beams Using S_0 Lamb Mode," *Composites Science and Technology*, Vol. 68, No. 6, 2008, pp. 1548-1554.

20. Guo, N. and Cawley, P., "The Interaction of Lamb Waves with Delaminations in Composite Laminates," *Journal of the Acoustical Society of America*, Vol. 94, No. 4, 1993, pp. 2240-2246.